I&EC research
Industrial & Engineering Chemistry Research

pubs.acs.org/IECR
Article

Fluid Dynamics of an Electrochemical Flow Reactor with Different Gas Diffusion Electrodes for In Situ Hydrogen Peroxide Production

Larissa Pinheiro de Souza, Isabela Matos Gaudio de Souza, Robson S. Souto, Matheus Schiavon Kronka, Bruno Ramos, Marcos R. V. Lanza, José Luís de Paiva, and Antonio Carlos Silva Costa Teixeira*

Cite This: *Ind. Eng. Chem. Res.* 2024, 63, 18053−18066

ABSTRACT: This study integrates macromixing and micromixing methodologies to characterize an electrochemical reactor with a gas diffusion electrode (GDE) based on computational fluid dynamics (CFD) simulations validated by residence time distribution (RTD) data. It experimentally evaluates two types of GDEs for H_2O_2 accumulation and uses the validated CFD model to evaluate the distribution of H_2O_2 in the reactor. The tanks-in-series (T-I-S) model provides a qualitative understanding of the fluid's macroscopic behavior, while the transition SST model analyzes the fluid's microscopic dynamics and turbulence zones. The study reveals a significant convergence of current density, volumetric flow rate, and GDE type for H_2O_2 production. The optimal experimental configuration (carbon/PTFE/fabric with $Q = 50$ L h^{-1}) was evaluated through CFD simulations in the distribution of H_2O_2 at different flow rates. These results improve our understanding of the hydrodynamics of the electrochemical reactor and offer prospects for optimizing the H_2O_2 generation and accumulation processes.

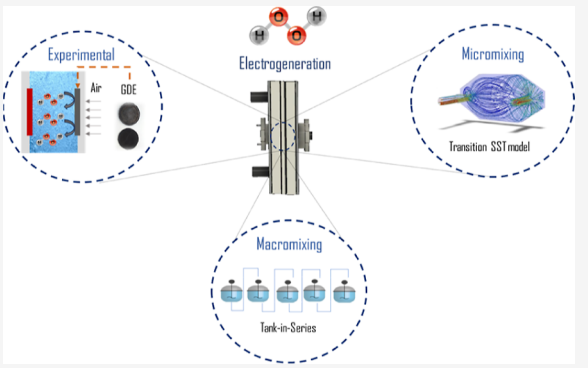

1. INTRODUCTION

Hydrogen peroxide (H_2O_2) plays an important role in different industrial sectors for oxidative applications as it is considered a powerful and environmentally friendly chemical oxidizer. The annual global consumption of this chemical is in the order of millions of tons, growing consistently year after year due to the versatility of its use in paper blanching, organic synthesis, and food disinfection, among other sectors.[1,2] More recently, H_2O_2 has also shown efficient application as a vital component in surface disinfection in response to the COVID-19 pandemic.[1,3,4] Furthermore, according to the literature, H_2O_2 is also highly efficient in the treatment of wastewater through advanced oxidative processes as one of the main precursors of hydroxyl radicals.[1,5]

The electrochemical production of H_2O_2 in situ through the oxygen reduction reaction (ORR) has been widely studied in wastewater treatment processes due to its advantages compared to the conventional production by the anthraquinone oxidation (AO) process.[6] The AO method, which is widely used for industrial-scale H_2O_2 production, involves substantial energy consumption, generates hazardous waste materials, and incurs substantial storage and transportation costs.[7]

The electrochemical approach to H_2O_2 synthesis can be based on either cathodic or anodic reactions. At the anode, the reaction, shown in eq 1, occurs with a remarkably low efficiency. Conversely, the cathodic ORR can yield two main products: H_2O_2, involving a two-electron transfer process (eq 2), or H_2O, through a four-electron transfer (eq 3).

$$2H_2O \rightarrow H_2O_2 + 2H^+ + 2e^- \qquad (E^0 = 1.76 \text{ V vs SHE}) \tag{1}$$

$$O_2 + 2H^+ + 2e^- \rightarrow H_2O_2 \qquad (E^0 = 0.69 \text{ V vs SHE}) \tag{2}$$

$$O_2 + 4H^+ + 4e^- \rightarrow 2H_2O \qquad (E^0 = 1.22 \text{ V vs SHE}) \tag{3}$$

Highly selective production of H_2O_2 from the ORR was achieved using electrodes made from carbon materials such as graphite, graphene oxide, carbon black, etc. These materials are widely adopted to produce H_2O_2 due to their favorable cost-effectiveness, large surface areas, functional surface groups, and inherent stability.[8] On the other hand, a typical shortcoming associated with carbon-based materials as electrochemical catalysts lies in their poor charge transfer capability, which leads to high overpotentials for H_2O_2 production and thus

Received: June 17, 2024
Revised: September 30, 2024
Accepted: October 4, 2024
Published: October 11, 2024

https://doi.org/10.1021/acs.iecr.4c02264
Ind. Eng. Chem. Res. 2024, 63, 18053−18066

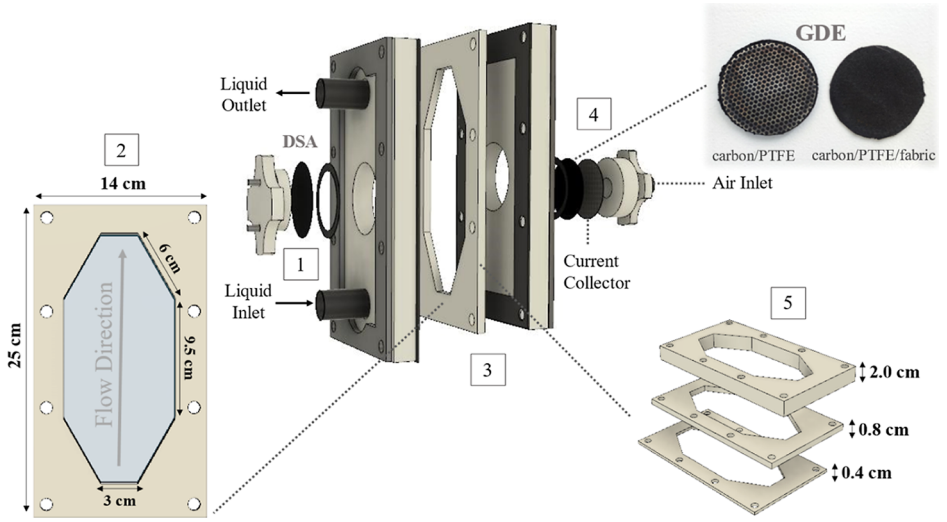

Figure 1. Schematic of the electrochemical reactor design equipped with a gas diffusion electrode (GDE). (1) Anode compartment (DSA: dimensionally stable anode); (2) dimensions of the reactive area and flow direction; (3) electrochemical reactor compartments; (4) gas diffusion electrode (GDE) compartment and electrodes (carbon/PTFE and carbon/PTFE/fabric); (5) interelectrode gaps.

higher energy consumption. Various strategies for modifying these materials have demonstrated efficient performance in favor of increasing their electron transfer efficiency. The literature reports successful studies involving the use of heteroatoms, metal oxides, noble metal nanoparticles, metal−organic frameworks (MOF), and metal coordination complexes.[9] In addition to being highly selective toward H_2O_2 production, amorphous carbon catalysts such as Printex L6 carbon (PL6C) or modified PL6C have proven to be very interesting for H_2O_2 production via a gas diffusion electrode (GDE) setup.[10,11]

The GDE design provides higher current efficiency for ORR in electrochemical processes, thanks to the porous structure that makes O_2 gas available at the catalytic surface via a three-phase interface (gas/electrode/electrolyte). Thus, restrictions on the slow kinetics of O_2 mass transport become negligible, making this electrode structure particularly suitable for H_2O_2 production under more realistic conditions[12,13] and highly applicable as an environmental technology for removing contaminants.[5,14−17] However, scaling up processes for the electrochemical production of H_2O_2 in flow reactors has been a challenge due to the complexities faced in GDE design. Therefore, the efficiency of H_2O_2 electrosynthesis will increasingly rely on integrated studies on catalyst properties and reactor designs that lead to optimal selectivity and overall yield.[18]

A key point of such integrated studies is a comprehensive understanding of fluid dynamics, which depends on the design of the equipment (such as a parallel plate, tubular, and filter press, among others) and is essential to a rational optimization of the system efficiency. Notably, the plane parallel configuration remains the most common choice of electrode geometry in applied electrochemistry and electrochemical engineering due to its numerous advantages, including diverse electrode shapes and materials, uniform potential and current distributions, easy scalability, flexible cell architecture, well-defined fluid flow and mass transfer, and the option of scaling up the process by increasing the number or area of the electrode.[19] The hydrodynamic characterization primarily involves the evaluation of residence time distribution (RTD), a widely used stimulus−response concept in the investigation and design of traditional chemical reactors.[20] RTD measurements facilitate the characterization of hydrodynamic behavior under specific operating conditions, offer insights into macromixing, and help diagnose flow pattern issues in nonideal reactors.[21,22] This diagnostic method can be applied for a global understanding of fluid behavior throughout the reactor or by directly obtaining stimulus−response measurements.[23]

Although this methodology has been widely applied in electrochemical reactors,[21−29] studies dealing with gas diffusion electrodes (GDEs) remain limited in the literature, especially those focusing on the in situ generation of H_2O_2.[6,30−32] Along with RTD and macromixing models, micromixing models, i.e., the study of mixing and transport processes on a molecular or microscopic scale within fluid elements, greatly increase the understanding of hydrodynamics, the reaction environment, and reactor performance.[33] The most common framework for carrying out micromixing simulations is computational fluid dynamics (CFD).[34] While macroscopic properties are typically determined using dispersion coefficients or by subdividing the reaction volume (i.e., the volume between the anode and cathode) into a series of ideal reactors, the flow field can be verified using numerical solutions to gain comprehensive insights into the effects of the reactor's structural details.

Therefore, the objective of this study is to discuss a connection between macromixing and micromixing methodologies to characterize an electrochemical flow reactor using a gas diffusion electrode (GDE) based on residence time distribution (RTD) data. In addition, we intended to evaluate two types of GDEs with respect to H_2O_2 accumulation along with hydrodynamic evaluation through computational fluid dynamics (CFD) simulations. As an alternative to the detailed treatment of this complex electrochemical system, due to the three-phase nature of the porous gaseous diffusion electrode, the CFD simulations discussed in our work focused on understanding the distribution of H_2O_2 inside the reactor, considering a simplified approach based on adopting an H_2O_2 source to represent its electrogeneration. The work therefore aims to provide important information about the significant relationship between the design of efficient reactors and

https://doi.org/10.1021/acs.iecr.4c02264
Ind. Eng. Chem. Res. 2024, 63, 18053−18066

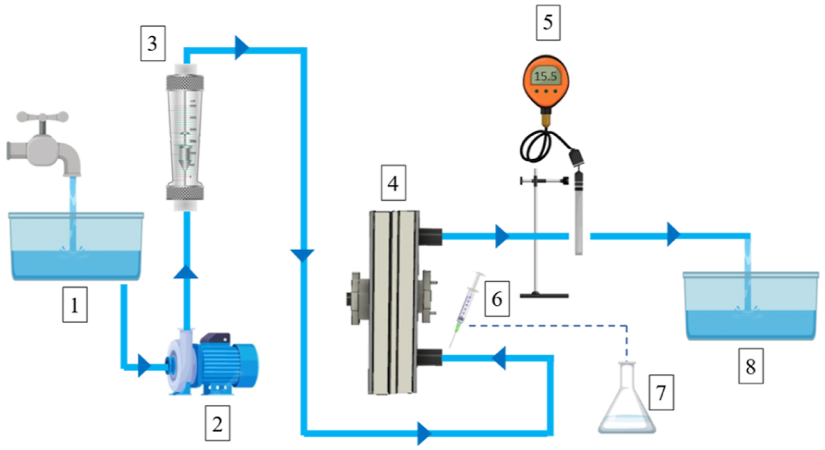

Figure 2. Experimental apparatus used in the RTD experiments. (1) Transport fluid (tap water tank); (2) centrifugal pump; (3) rotameter; (4) electrochemical flow reactor; (5) in-line conductivity meter; (6) pulse injection syringe; (7) tracer stock solution; (8) waste tank.

electrosynthesis systems in electrochemical environmental engineering studies.

2. MATERIALS AND METHODS

2.1. Chemicals. Sodium sulfate (Na_2SO_4 99%, Vetec), hydrochloric acid (HCl 36.5−38%, Vetec), and sodium hydroxide (NaOH 99%, Vetec) were used to prepare electrolytes and adjust the pH. Potassium chloride (KCl 99%, Quimica Moderna) was used as a tracer in the RTD experiments. To quantify hydrogen peroxide (H_2O_2), a solution was prepared using sulfuric acid (H_2SO_4 95−98%, Synth) and ammonium molybdate ($(NH_4)_6Mo_7O_{24}$ 81−83%, Synth), as reported in the literature.[35]

2.2. Gas Diffusion Electrode Synthesis. The GDE synthesis procedure was adapted from literature.[35] Commercial carbon black Printex L6 (CPL6), purchased from Evonik, was used as the diffusion layer for the electrode structure. CPL6 was mixed with poly(tetrafluoroethylene) (PTFE), a 60% aqueous dispersion, purchased from Dupont (USA) in a ratio of 80:20 (w/w). A quantity of 8 g of this mixture was stirred for 40 min and was then vacuum-filtered for 15 min to remove excess water. The paste obtained was further compressed between two metal mesh plates with a geometrical area of 20 cm^2 at 290 °C for 2 h using 11 tons of pressure, resulting in a material with an area density of 400 mg cm^{-2}. To improve the GDE synthesis methodology, the same mixture was used in a different setup with a lower area density (23 mg cm^{-2}). This methodology is described in ref 36, in which 3 g of the carbon/PTFE mixture (catalytic mass) was deposited on a commercial conductive carbon fabric with a geometric surface area of 126 cm^2, purchased from ZOLTEK. Finally, the assembly (fabric and carbon paste mixture) was hot-pressed at 290 °C for 15 min using 4.5 tons of pressure. Finally, the electrodes were cut to a geometric surface area of 20 cm^2.

2.3. Electrochemical Reactor Design. Figure 1 illustrates the configuration of the electrochemical flow reactor used in the H_2O_2 electrogeneration tests, featuring its internal dimensions, flow direction, and electrode compartments. The two GDEs described above were synthesized and used as the cathode, while the anode was a dimensionally stable RuO_2−TiO_2 anode (DSA−Cl_2, De Nora do Brasil) with an exposed area of 20 cm^2. The schematic also provides specific information on the interelectrode gaps used (0.4, 0.8, and 2.0 cm) (Figure 1 (5)), which directly affect the internal volume of the reactor (177.5, 225, and 390 mL, respectively).

2.4. RTD Characterization and Macroscopic Approaches for Flow under Nonideal Conditions. The residence time distribution (RTD) experiments were carried out in the reactor shown in Figure 1. The tests involved varying the liquid flow rate by two levels (Q = 30 and Q = 50 L h^{-1}) and the interelectrode gaps (IEGs) by three levels, as illustrated in Figure 1. These variations resulted in the following volumes of the system (IEG + tubing): (1) (IEG_1, V_1 = 187.5 mL), (2) (IEG_2, V_2 = 235 mL), and (3) (IEG_3, V_3 = 400 mL). The tests used the tracer pulse methodology, which consists of introducing a tracer pulse at the reactor inlet through which a constant and stable flow of inert fluid passes and continuously tracking its presence as it passes through the system until it reaches the detector, as depicted in Figure 2. A pulse of 1 mL of the tracer solution (concentrated potassium chloride solution $[KCl]_0$ = 3 mol L^{-1}) was injected for 1 s at a time into the reactor inlet using a syringe, and its concentration was monitored over time by conductivity measurements at the reactor outlet using an in-line electrical conductivity meter (Instrutherm CD-850) (Figure 2). A centrifugal pump (BOMAX NH-30PX-T) was used to drive the inert fluid (water). The flow rate was adjusted using a needle valve and was read using a rotameter. The experiments were carried out at free pH (~7.0) and in triplicate, i.e., three complete tests were carried out for each flow rate and IEG.

The tracer concentration measured over time was used to calculate the residence time distribution in terms of the *exit-age distribution function* ($E(t)$). The function is given by eq 4, respectively

$$E(t) = \frac{C(t)}{\int_0^\infty C(t)\,dt} \tag{4}$$

From the calculation of the residence time distribution, it was possible to determine the mean residence time (t_m)

$$t_m = \frac{\int_0^\infty tE(t)\,dt}{\int_0^\infty E(t)\,dt} = \int_0^\infty tE(t)\,dt \tag{5}$$

Based on $E(t)$ and t_m, the variance (σ^2) and skewness (s^3) of the distribution can also be determined

https://doi.org/10.1021/acs.iecr.4c02264
Ind. Eng. Chem. Res. 2024, 63, 18053−18066

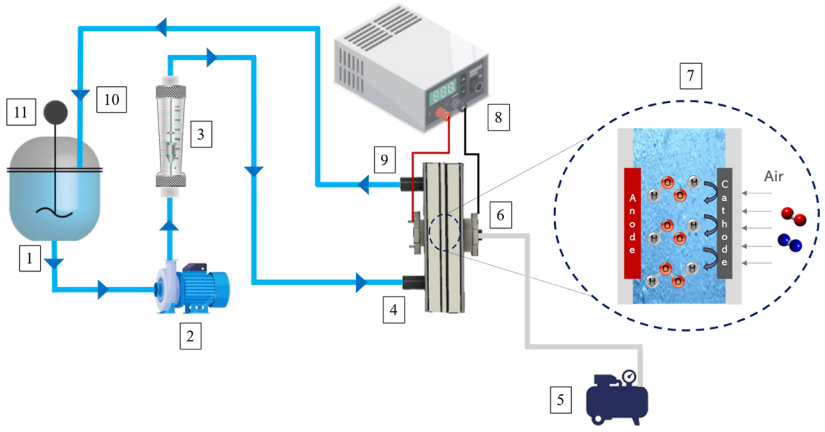

Figure 3. H_2O_2 electrogeneration configuration. (1) Solution vessel; (2) centrifugal pump; (3) rotameter; (4) reactor solution inlet; (5) air compressor; (6) air inlet; (7) formation of H_2O_2 on the surface of the air-fed cathode (GDE); (8) power supply; (9) reactor solution outlet; (10) recirculation vessel inlet; (11) vessel impeller.

$$\sigma^2 = \int_0^\infty (t - t_m)^2 E(t)\, dt \tag{6}$$

$$s^3 = \frac{1}{\sigma^{3/2}} \int_0^\infty (t - t_m)^3 E(t)\, dt \tag{7}$$

To assess the ideality of the flow distribution, the space time (τ), defined as the ratio between the reactor volume (L) and the flow rate (L h^{-1}), is also calculated

$$\tau = \frac{V}{Q} \tag{8}$$

The following three nonideality indices based on relationships between space time (τ), peak time (t_p), and mean residence time (t_m) were calculated using the RTD profiles[20,37]

$$\text{plug flow index} = \frac{t_p}{\tau} \tag{9}$$

$$\text{dead zone index} = \frac{t_m}{\tau} \tag{10}$$

$$\text{short circuiting index} = 1 - \left(\frac{t_p}{t_m}\right) \tag{11}$$

From this perspective, integrating RTD characterization data with a macroscopic model offers a reasonable approach to improving our understanding of the flow behavior inside the electrochemical reactor. Among the variety of models detailed in the literature, this study focuses on those that have gained prominence,[20,34] including

1 The *laminar flow reactor* (LFR) model, characterized by a single parameter (t_m), which assumes a laminar flow pattern inside the reactor

$$E(t) = \begin{cases} 0 & t < \dfrac{t_m}{2} \\ \dfrac{t_m^{\,2}}{2t^3} & t \geq \dfrac{t_m}{2} \end{cases} \tag{12}$$

2 The *tanks-in-series* (T-I-S) model, which divides the total volume into $N = \frac{t_m^2}{\sigma^2}$ perfectly mixed stirred tanks, each with a capacity equivalent to t_m

$$E(t) = \left(\frac{t}{t_m}\right)^{N-1} \frac{N^N}{(N-1)!} e^{-tN/t_m} \tag{13}$$

3 The *series-connected CSTR+PFR* model, which represents the real reactor as a combination of a continuous stirred tank reactor (CSTR) coupled to a plug flow reactor (PFR), where the total volume is divided equally between the two ideal reactors, with $t_m = \tau_{CSTR} + \tau_{PFR}$

$$E(t) = \begin{cases} 0 & t < \tau_{PFR} \\ \dfrac{e^{-(t-\tau_{PFR})/\tau_{CSTR}}}{\tau_{CSTR}} & t \geq \tau_{PFR} \end{cases} \tag{14}$$

4 The *axial dispersion* (AD) model, which quantifies the dispersion of material in the reactor in relation to the Peclet number (Pe) and t_m, considering the velocity (u), reactor length (L), and diffusivity (D)

$$\frac{\sigma^2}{\tau^2} = \frac{2}{Pe} + \frac{8}{Pe^2} \tag{15}$$

$$E(t) = \sqrt{\frac{u^3}{4\pi DL}}\, e^{\left[-(L-ut)^2/\frac{4DL}{u}\right]} \tag{16}$$

2.5. Electrogeneration of H_2O_2 Using a Gas Diffusion Electrode. Figure 3 shows the configuration of the electrochemical reactor for H_2O_2 electrogeneration in batch operation with liquid recirculation. The reactor outlet is connected to the reservoir, which is connected to a centrifugal pump (BOMAX NH-30PX-T), recirculating 1 L of the electrolyte solution ($[Na_2SO_4]_0$ = 0.1 mol L^{-1} at pH = ~3.0). This electrolyte concentration was selected to reflect the conductivity values typically found in wastewater. The liquid flow rates (30 and 50 L h^{-1}) were adjusted using a needle valve and read using a rotameter. An air compressor (Comp-1, Wimpel) regulated by a manometer provided a gas pressure (P = 0.2 bar) sufficient to keep the gas flow rate to the GDE constant and equal to 50 mL min^{-1}, as controlled by a rotameter. Electrolysis was carried out using a power supply (PS-6100, Icel Manaus) with different current densities (j) (33 to 96 mA cm^{-2}) to evaluate the accumulation of H_2O_2 in the reactor. For the anode, a dimensionally stable anode−chlor alkali (DSA−Cl_2) was used

https://doi.org/10.1021/acs.iecr.4c02264
Ind. Eng. Chem. Res. 2024, 63, 18053−18066

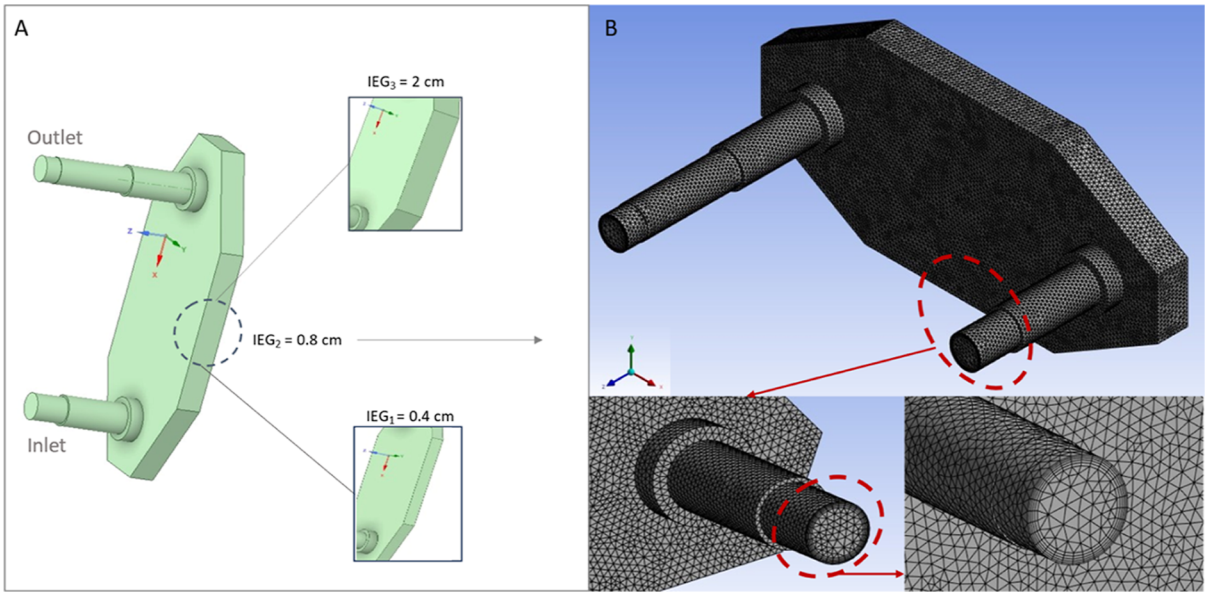

Figure 4. Side and internal views of a representative geometry and mesh used to discretize the electrochemical flow reactor. (A) depicts the three different geometries, while (B) illustrates a typical mesh for IEG = 0.4 cm.

(with an exposed area of 20 cm^2, from De Nora do Brasil) with the same geometric area as the synthesized cathodes.[38]

H_2O_2 quantification was carried out using 0.5 mL samples collected in the vessel at various time points during the 60 min assay. Following a procedure described in the literature,[2] these samples were introduced into 4 mL of ammonium molybdate solution with a concentration of $[(NH_4)_6Mo_7O_{24}]_0 = 2.4 \times 10^{-3}$ mol L^{-1}, which forms a complex detectable in the UV spectrum with an absorption peak at 350 nm. These solutions were then analyzed by using a UV−vis spectrophotometer (Varian Cary 50). The quantified H_2O_2 was employed to analyze the electrochemical efficiency of the reactor system using specific parameters, such as current efficiency (eq 17) and energy consumption (eq 18)[6]

$$\mathrm{CE}_{H_2O_2}(\%) = \frac{2FC_{H_2O_2}V_e}{It_c} \times 100 \tag{17}$$

$$\mathrm{EC}(\mathrm{kW\,h\,kg^{-1}}) = \frac{1000EIt_c}{V_eC_{H_2O_2} \times 3600} \tag{18}$$

where the value 2 denotes the transfer of electrons for the reduction of O_2; F represents the Faraday constant (96,487 C mol^{-1}); $C_{H_2O_2}$ is the concentration of H_2O_2 (mol L^{-1} for CE and mg L^{-1} for EC); V_e (L) is the electrolyte volume; I (A) is the current passing through the cathode at time t_c (s); and E (V) is the cell potential.

The H_2O_2 production capacity was also quantified in terms of space-time yield (Y_{ST}) using eq 19

$$Y_{ST}(\mathrm{g\,L^{-1}\,h^{-1}}) = \frac{3600ajCEM}{nF1000} \tag{19}$$

where a denotes the specific electrode surface (m^2 m^{-3}), which is determined by dividing the electrode area by the reactor volume; j is the current density (A m^{-2}); CE stands for the current efficiency; n corresponds to the number of electrons participating in the reduction reaction; F is Faraday's constant (96,485 C mol^{-1}); and M is the molar weight of H_2O_2 (g mol^{-1}).

2.6. Flow Field Analysis Using Computational Fluid Dynamics (CFD). The simulations were carried out on a CFD model of the reactor using an ANSYS Fluent 2023 R2. Three geometries were constructed in the ANSYS SpaceClaim to represent the three internal volumes (187.5, 235, and 400 mL) investigated (Figure 4A) and were discretized in ANSYS Meshing using tetrahedral meshes with a maximum of 5 inflation layers placed along the walls to ensure adequate boundary layer resolution (Figure 4B). The mesh convergence was monitored using the mean residence time (t_m) calculated by a sensitivity analysis (Figure S1). The flow field in the reactor was simulated under coupled pressure-based solver type, absolute velocity formulation, and steady-state conditions for two flow rates (30 and 50 L h^{-1}). The convergence of the numerical solution was verified by monitoring the maximum of the normalized residuals of the equations, which reached a value of less than 10^{-4} with low computational cost. Calculation times ranged from 2 to 5 min using the computing power of the Intel(R) Core(TM) i5-6400 CPU, supported by 16 GB of RAM, all operating in the Windows 10 Pro environment.

2.6.1. RTD Predictions. To provide a more accurate description of the hydrodynamic characteristics, the experimental RTD assays were complemented by a CFD numerical simulation of RTD to identify the most suitable micromixing model to represent the system. Initially, simulations were carried out using the laminar flow model, and their results served as initial conditions for the turbulent models selected: k−omega (k−ω), transition SST (SST), and Reynolds stress (RSM).

The most common CFD strategy for investigating micromixing uses the finite-volume method to numerically solve the Reynolds-averaged Navier−Stokes (RANS) equation. The flow field can be determined by numerically solving eqs 20 and 21. In eq 21, the effects of turbulence are represented by the term $-\rho\overline{u_i'u_j'}$, referred to as the Reynolds stress.[39]

$$\frac{\partial \overline{u}_i}{\partial x_i} = 0 \tag{20}$$

https://doi.org/10.1021/acs.iecr.4c02264
Ind. Eng. Chem. Res. 2024, 63, 18053−18066

$$\frac{\partial \overline{u_i}}{\partial t} + u_j \frac{\partial \overline{u_i}}{\partial x_j} = -\frac{1}{\rho}\frac{\partial P}{\partial x_i} + \frac{\partial}{\partial x_j}\left(\mu \frac{\partial \overline{u_i}}{\partial x_j} - \overline{u_i' u_j'}\right) \quad (21)$$

where ρ is the density, μ is the viscosity, P is the pressure, $\overline{u_i}$ is the mean velocity, u_i' is the fluctuating velocity, and $u_i = \overline{u_i} + u_i'$ is the local velocity in the ith direction.

To model the effects of turbulence, several approaches can be used, each offering a balance between accuracy and computational cost. The $k-\omega$ ($k-\omega$) model is particularly effective at capturing near-wall effects and flows with adverse pressure gradients. It solves two transport equations: one for the turbulent kinetic energy (k) and one for the specific dissipation rate (ω). The turbulent viscosity (μ_t) is calculated using eq 22

$$\mu_t = \frac{\rho k}{\omega} \quad (22)$$

The transition SST model is a variation of the $k-\omega$ model that combines the best aspects of the $k-\varepsilon$ and $k-\omega$ models with a smooth transition between the two, which makes it especially useful for predicting flow separation in low- and high-Reynolds number conditions. Turbulent viscosity is also determined using k and ω, but with a formulation that improves the prediction of separated flows[39]

$$\mu_t = \min\left(\frac{\rho k}{\omega}, \frac{\rho \alpha_1 k}{\max(\alpha_1 \omega, SF_2)}\right) \quad (23)$$

where α_1 is a model constant and S and F_2 represent the strain rate of the flow and a blending function, respectively.

On the other hand, the Reynolds stress model (RSM) offers a more sophisticated approach by directly solving the Reynolds stresses ($\tau_{ij} = -\rho \overline{u_i' u_j'}$) rather than assuming isotropy in the turbulence. In this model, turbulent viscosity is less prominent as the transport equations for the Reynolds stress components replace the equations for k and ω. The Reynolds stresses are obtained by solving transport equations that consider the production, dissipation, and diffusion of turbulence, providing a more accurate description of anisotropic and complex effects of turbulent flow.

In addition, in this work, a discrete phase model was employed to introduce massless tracers into the inlet, and their trajectories were tracked using the Lagrangian method.[39−41] These tracers, small particles with a diameter of 1 μm and the same density as that of the liquid, were designed to follow the flow pattern. The random walk model[39] was employed to calculate how the tracers dispersed due to turbulent eddies, introducing random variations in the local mean flow. The key equations involved are[39−41]

$$\frac{dx_p}{dt} = u \quad (24)$$

$$v_p = u \quad (25)$$

where x_p is the particle position vector, t is the time, u is the velocity of the fluid (continuous phase), and v_p is the particle velocity.

Important parameters for accurate RTD calculations were established, including the number of tracers (set to 5000) and time steps (set to 5).[42] The boundary conditions were specified as the magnitude of the velocity at the inlet and gauge pressure at the outlet (detailed values are given in Table S1). The boundary conditions for the wall were defined as stationary walls with no-slip conditions. Finally, the evaluation was based on monitoring the time required for the tracers to travel from the inlet to the outlet of the reactor. The residence times recorded for all of the tracers were then aggregated to derive a residence time distribution and calculate the mean residence time.

2.6.2. H_2O_2 Injection into the Flow Field. CFD numerical simulations, considering the injection of H_2O_2 at a hypothetical point at the reactor inlet (to simulate H_2O_2 recirculation) and in the electrode surface (to simulate H_2O_2 production), were conducted for both GDEs evaluated (Figure 5). The injections were made using the discrete phase model

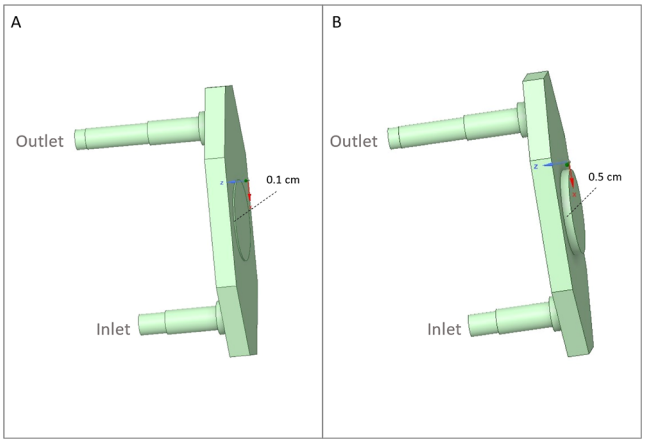

Figure 5. Representative geometries used for different gas diffusion electrodes (GDEs) with the corresponding thickness of the carbon mass indicated. (A) Carbon/PTFE/fabric; (B) carbon/PTFE.

to introduce H_2O_2 as an inert substance (hydrogen peroxide liquid), and its properties were retrieved from the ANSYS Fluent library.[39] The mass flow rates (kg s^{-1}) of added H_2O_2 were calculated based on mass balances using experimental data and were incorporated into the simulations (Table S2). The simulations were conducted using previously validated flow field boundary conditions for the continuous phase, as detailed in Section 2.6.1. The boundary conditions for H_2O_2 injections were specified as the velocity magnitude near the electrode surface region (detailed values are in Table S1), with identical conditions applied at the reactor inlet during H_2O_2 injection (Section 2.6.1). Finally, the treatment of H_2O_2 inert particles in Fluent was carried out considering interactions with the continuous phase and unsteady particle tracking.[42]

3. RESULTS AND DISCUSSION

3.1. Understanding the Flow Behavior in the Electrochemical Reactor. *3.1.1. Mesh Convergence Analysis.* Mesh convergence was examined in the complex velocity field observed for the simulated scenarios (laminar model and Q = 50 L h^{-1}) (Figure S1). The solutions were assessed using the response variable mean residence time (t_m), with variations of less than 8% for meshes exceeding 306,844 elements for IEG_1 (V_1 = 187.5 mL), 339,681 elements for IEG_2 (V_2 = 235 mL), and 420,099 elements for IEG_3 (V_3 = 400 mL) (Figure 4). The meshes had an average orthogonal quality of over 0.75 with skewness values below 0.2, ensuring the accuracy of the calculation results. Similar results regarding mesh orthogonal quality and skewness have been reported in the discretization

https://doi.org/10.1021/acs.iecr.4c02264
Ind. Eng. Chem. Res. 2024, 63, 18053−18066

Table 1. RTD Parameters of the Electrochemical Reactor

Q (L h^{-1})	V (mL)	τ (min)	t_m (min)	σ^2 (min)^2	s^3 (min)^3	$t_m - \tau$ (min)	t_p/τ	t_m/τ	$1 - (t_p/t_m)$
50	187.5	0.225	0.247	0.074	0.459	0.022	0.800	1.100	0.270
	235.0	0.282	0.338	0.024	0.156	0.056	0.890	1.200	0.260
	400.0	0.480	0.520	0.027	0.083	0.040	0.770	1.080	0.290
30	187.5	0.375	0.361	0.040	0.217	−0.014	0.720	0.960	0.250
	235.0	0.470	0.588	0.117	0.465	0.118	0.830	1.250	0.340
	400.0	0.800	1.034	0.228	0.503	0.234	0.840	1.390	0.350

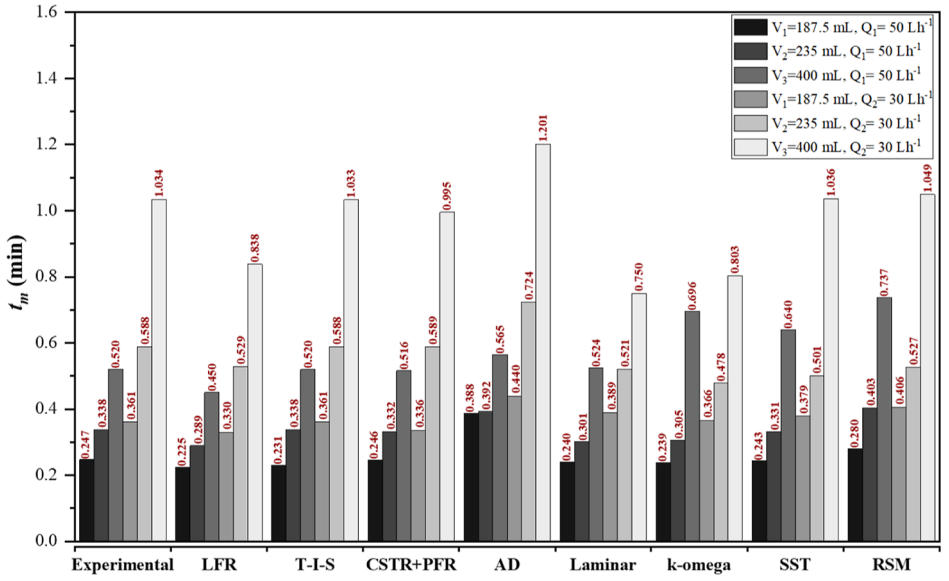

Figure 6. Evaluation of experimental data using macroscopic and microscopic approaches to characterize the flow of the electrochemical reactor by predicted mean residence times (t_m).

of a parallel-plate electrochemical reactor geometry,[43] which validate our findings. Consequently, these mesh densities were used to simulate the RTD as the simulations did not present convergence issues with turbulence models, and the computational costs were not significantly high.

3.1.2. Validation of Macromixing and Micromixing Models through RTD Experiments. Table 1 shows the various parameters evaluated using the data from the RTD experiments conducted at different flow rates. In general, a pattern with fewer nonideality conditions is observed, particularly evident in the ($t_m - \tau$) values, when comparing Q = 50 L h^{-1} with Q = 30 L h^{-1}. At 50 L h^{-1}, it is worth noting that, for V = 235 mL, we observe a behavior with low variance (σ^2 = 0.024), fewer short circuits $\left(1 - \left(\frac{t_p}{t_m}\right) = 0.26\right)$, and greater similarity to plug-flow $\left(\frac{t_p}{\tau} = 0.89\right)$ behavior. This observation suggests that, despite the presence of dead zones ($\frac{t_m}{\tau} = 1.2$), this scenario aligns more closely with ideal flow conditions, providing the optimum t_m among the three scenarios evaluated at this flow rate. At a flow rate of 30 L h^{-1}, a volume of 187.5 mL showed the most ideal behavior. The low variance (σ^2 = 0.0400) suggests minimal dispersion, leading to a more concentrated residence time distribution. With $\frac{t_p}{\tau} = 0.72$ and $\frac{t_m}{\tau} = 0.96$, the system shows a reasonable approximation to the plug flow with few dead zones. The low short-circuit index (0.25) also indicates a minimal fluid bypass, making this configuration optimal for obtaining a more uniform flow.

The work of ref 44 reported comparable results of RTD parameters for an electrochemical reactor, where an intermediate flow rate resulted in the lowest formation of nonideality zones. The authors also emphasized the importance of a low variance (σ^2) value for the efficiency of the electrochemical reactor.

The RTD experimental data was used to validate the macromixing and micromixing models in the reactor, as shown in Figure 6. The mean experimental residence times for the scenarios considered ranged from 0.225 to 1.201 min. From a microscopic model perspective, laminar, $k-\omega$ ($k-\omega$), transition SST (SST), and Reynolds stress (RSM) were chosen to characterize the regime.

The investigation of the flow dynamics in the reactor involved the application of four macroscopic models of nonideality (Section 2.4). The LFR model predicted shorter mean residence times compared to the experimental values, accompanied by pronounced residuals, indicating its inadequacy to account for the local turbulence-related phenomena. The adjusted Peclet (Pe) numbers for the AD model ranged from 9 to 13, exceeding the corresponding experimental values. Consequently, both the LFR and AD models failed to faithfully reproduce the experimental behavior (Figure 6). In contrast, the CSTR + PFR model suggested that the electrochemical reactor behaves as a combination of a continuous stirred tank reactor (CSTR) and a plug flow reactor (PFR) in series with the total reactor volume divided equally between the two ideal reactors. Conversely, the T-I-S model postulated an equivalence between the electrochemical reactor and 3−5 CSTRs of identical sizes. Although the CSTR + PFR model reproduced

https://doi.org/10.1021/acs.iecr.4c02264
Ind. Eng. Chem. Res. 2024, 63, 18053−18066

the experimental data well, it was evident that mixing effects predominated over the plug flow profile. This observation led to the selection of the T-I-S model as the preferred macroscopic model to describe this system, given its exceptional capacity to accurately represent the experimental data and mean residence times within the experimental space explored, as shown in Figure 6. Comparable results from a macroscopic perspective were observed in ref 6, in which the combination of CSTR + PFR was found to best describe the phenomena in the flat plate electrochemical reactor. The influence of the PFR can be explained by the internal geometry of the reactor, which directed the flow toward the electrodes. Therefore, owing to its minimal residuals and heightened capability to capture mixing effects, the T-I-S model stands as the most suitable macroscopic model for delineating fluid flow phenomena within the electrochemical reactor evaluated.

The computational micromixing models were able to accurately replicate the experimental RTD data (Figure 6), with the SST model performing particularly well at a flow rate of 50 L h^{-1}, as demonstrated by a classic experimental RTD curve (Figure 7A). Although these classical RTD results

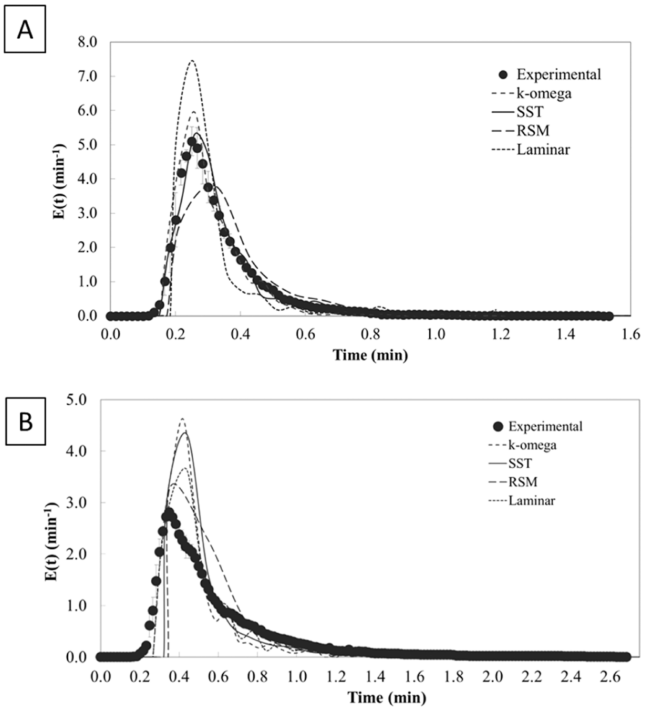

Figure 7. Evaluation of computational flow models using RTD data for a reactor volume of 235 mL at flow rates of (A) 50 and (B) 30 L h^{-1}.

provide a global understanding of the flow behavior inside the reactor, the experimental values matched well with those obtained in the simulations. It is worth mentioning that the RTD curves obtained using image processing techniques from a transparent frame can offer even more reliable comparisons, as discussed in ref 23.

In a high-flow scenario (Q = 50 L h^{-1}), it can be seen that the transition SST (SST) model is the most suitable for describing the regime. This model can accurately describe flows in environments with turbulence zones.[45] In this case, the recirculation zones are concentrated at the inlet and outlet due to the higher velocity fields generated (Figure 8A). Conversely, at a low flow rate (Q = 30 L h^{-1}), a behavior closer to laminar or RSM is observed (Figure 7B). A larger stagnation zone is noticeable at the reactor inlet, followed by additional dead zones (Figure 8B). These stagnation zones are accurately represented by the RSM model given its robustness and ability to describe complex flows effectively. This model can solve the Navier−Stokes equations using Reynolds averaging and rigorously considers the effects of swirl, rotation, and variations in strain rates.[45] In contrast, the $k-\omega$ turbulence model struggled to accurately depict the experimental data in both scenarios (Figure 7). This observation can be attributed to the fact that this type of turbulence model considers turbulence characteristics by accounting for kinetic energy and energy dissipation rates, which are typically associated with the prevalence of turbulent regime zones with pronounced viscous effects.[45] In general, the magnitude of the average velocity observed near the midpoint of the electrode surface (ν = 0.0226 m s^{-1} for Q = 50 L h^{-1}; ν = 0.0146 m s^{-1} for Q = 30 L h^{-1}) is within the same order of magnitude as those reported in the literature for systems under similar conditions.[6,19]

3.2. Assessing H_2O_2 Electrogeneration and Accumulation with Different GDEs. Different current densities (j) were employed to evaluate the generation of H_2O_2 and the accumulation capacity of the reactor during 60 min under different conditions, including the application of two different gas diffusion electrodes (GDEs) (carbon/PTFE and carbon/PTFE/fabric) and two flow rates (Q_1 = 30 L h^{-1} and Q_2 = 50 L h^{-1}). For this analysis, a supporting electrolyte of $[Na_2SO_4]_0$ = 0.1 mol L^{-1} (pH = 3.0) was used, air was applied as the O_2 source, a dimensionally stable anode (DSA) was used, and the reactor temperature was maintained at a constant temperature (25 °C).

As depicted in Figure 9A, during the 60 min electrolysis period, there was a gradual increase in H_2O_2 concentration over time, which was more pronounced for the carbon/PTFE/fabric electrode at 50 L h^{-1} for both scenarios. The maximum concentrations achieved for this electrode were 145.4 and 152.4 mg L^{-1} for current densities of 46 and 59 mA cm^{-2}, respectively. However, within 96 mA cm^{-2}, there was a decline in the level of H_2O_2 accumulation, decreasing to 137.2 mg L^{-1}. At significantly lower concentrations but exhibiting a pattern similar to that of carbon/PTFE/fabric, maximum concentrations of 60.9 and 98.3 mg L^{-1} were observed for current densities of 33 and 46 mA cm^{-2}, respectively, using the carbon/PTFE electrode. However, at a current density of 59 mA cm^{-2}, a decrease in H_2O_2 accumulation was also observed, resulting in an ultimate concentration of 48.8 mg L^{-1}.

Recent studies have highlighted the substantial impact of both the catalytic nature and the synthesis method of these gas diffusion electrodes on H_2O_2 electrogeneration.[6,13,36,46] Notably, electrodes featuring catalytic mass deposited on fabric[6,13] exhibit significantly higher accumulations of H_2O_2 compared to conventional electrodes[36,46] operating under similar electrochemical conditions, validating the results obtained in this work.

By modifying the hydrodynamic conditions from Q_1 = 30 L h^{-1} to Q_2 = 50 L h^{-1} while keeping the same GDE (carbon/PTFE/fabric), we observed a substantial impact of the flow rate on H_2O_2 electrogeneration (Figure 9B). At Q_2 = 50 L h^{-1}, the maximum concentrations achieved were 145.4 and 152.4 mg L^{-1} for current densities of 46 and 59 mA cm^{-2}, respectively. However, when the current density was increased to 96 mA cm^{-2}, there was a decrease in H_2O_2 accumulation,

https://doi.org/10.1021/acs.iecr.4c02264
Ind. Eng. Chem. Res. 2024, 63, 18053−18066

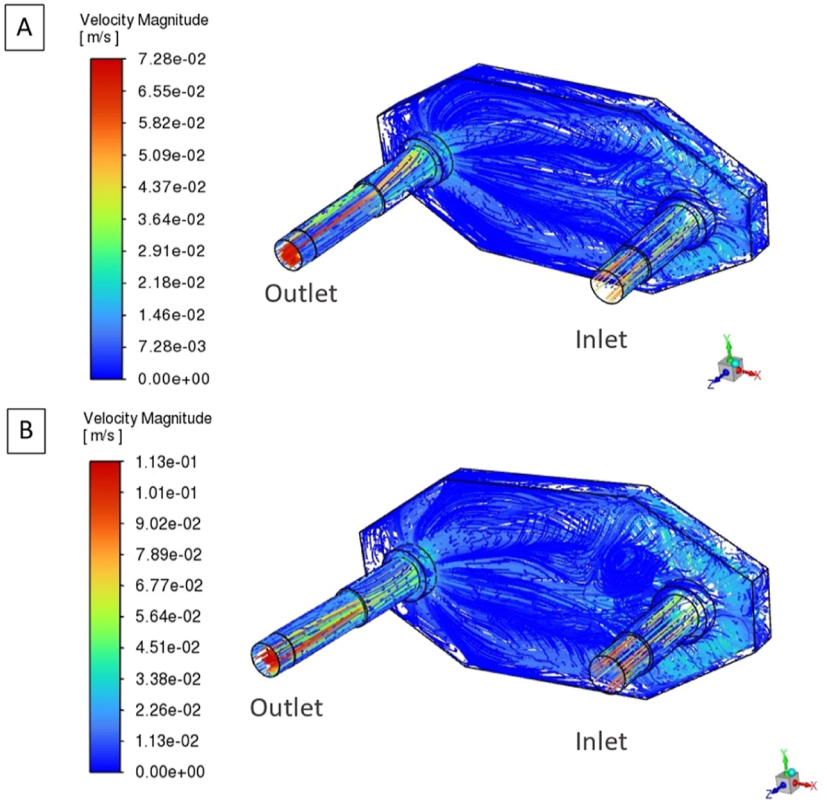

Figure 8. Evolution of the flow patterns inside the reactor, showing the magnitude of the liquid velocity with the transition SST model at (A) 50 and (B) 30 L h^{-1}.

falling to 137.2 mg L^{-1}. Conversely, when operating at a lower flow rate (Q_l = 30 L h^{-1}), a distinct behavior was observed. Here, the maximum concentration reached was 76.8 mg L^{-1} at a current density of 46 mA cm^{-2}. However, at current densities of 59 and 96 mA cm^{-2}, we again witnessed a decline in H_2O_2 accumulation, falling to 50.5 and 56.5 mg L^{-1}, respectively.

While the hydrodynamics of the system at 30 L h^{-1} result in a longer mean residence time (t_m = 0.588 min) compared to that at 50 L h^{-1} (t_m = 0.338 min), a lower accumulation of electrogenerated H_2O_2 was observed at the lower flow rate (Figure 9B). Possible explanations for this phenomenon are linked to the influence of the reduced velocity field, which causes increased formation of dead zones and preferential paths within the internal configuration of the reactor, as indicated by the RTD indices (Table 1) and CFD simulations (Figure 8). However, it is worth noting that the internal structure of the reactor with fluid direction plays a crucial role in mitigating the effects of nonideality, thus allowing for longer residence times conducive to greater H_2O_2 accumulation, as exemplified in the work in ref 6.

Typically, as the current density (j) increases, a greater accumulation of H_2O_2 is expected because more electrons become accessible in the system. Nevertheless, as j progressively increases, the occurrence of parallel reactions also increases. However, it is imperative to acknowledge that, in the absence of target reactants, the H_2O_2 concentration would not diminish; instead, it would stabilize at a level where the rates of both H_2O_2 production (eqs 2 and 3) and decomposition (via the anode surface, eq 26, and self-decomposition of H_2O_2, eq 27) would attain equilibrium at the anode.[47,48] Therefore, based on the experimental findings (Figure 9), it is clear that the decrease in H_2O_2 concentration can be attributed to its interaction with other concurrently electrogenerated oxidants during the electrochemical process, such as O_3 (eqs 28 and 29) and SO_5^{2-} (eqs 30–32) formed with DSA.[36]

$$H_2O_2 \rightarrow O_2 + 2H^+ + 2e^- \quad (26)$$

$$2H_2O_2 \rightarrow O_2 + 2H_2O \quad (27)$$

$$3H_2O \rightarrow O_3 + 3H^+ + 6e^- \quad (28)$$

$$H_2O_2 + O_3 \rightarrow 2O_2 + H_2O \quad (29)$$

$$H_2O + SO_4^{2-} \rightarrow 2H^+ + 2e^- + SO_5^{2-} \quad (30)$$

$$H_2O_2 + SO_5^{2-} \rightarrow 2O_2 + H_2SO_4 \quad (31)$$

$$O_3 + SO_5^{2-} \rightarrow 2O_2 + SO_4^{2-} \quad (32)$$

Another crucial aspect regarding the parallel reactions resulting from the increase in current density is the consequent effect on the four-electron reduction of oxygen, yielding H_2O as a product (eq 33), in addition to the hydrogen evolution reactions (eq 34)

$$O_2 + 4H^+ + 4e^- \rightarrow 2H_2O \quad (33)$$

$$2H^+ + 2e^- \rightarrow H_2 \quad (34)$$

It is important to note that when air serves as the oxygen source, the amounts of H_2O_2 generated tend to be lower compared to those obtained under similar hydrodynamic conditions with a pure O_2 supply.[15] However, the convenience of employing compressed air makes this technology more applicable in practice. Therefore, it follows that excessively

https://doi.org/10.1021/acs.iecr.4c02264
Ind. Eng. Chem. Res. 2024, 63, 18053−18066

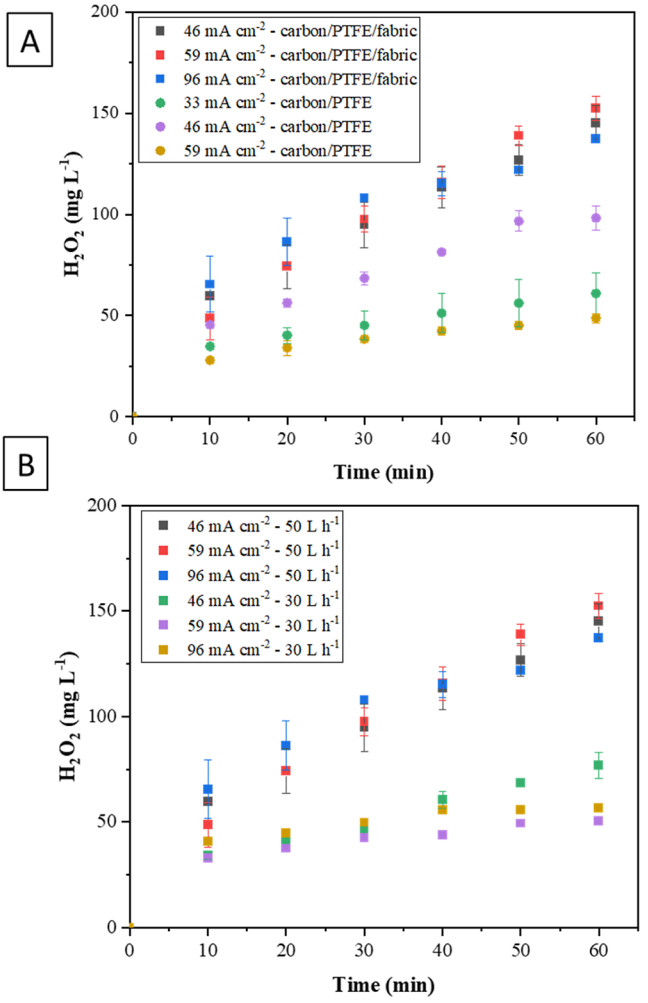

Figure 9. Accumulated H_2O_2 concentration over 60 min in the electrochemical reactor with electrogenerated H_2O_2 in situ. (A) Comparison of GDE at Q = 50 L h^{-1}; (B) comparison of flow rates with carbon/PTFE/fabric. $[Na_2SO_4]_0$ = 0.1 mol L^{-1}; pH = 3.0.

high current densities are not ideal for operations involving gas diffusion electrodes, highlighting the importance of identifying the optimal current density for each scenario.

The current efficiency, energy consumption, and space-time yield data obtained corroborate this observation. As shown in Figure 10, higher current efficiencies are linked to lower energy consumption and are intrinsically associated with the efficiency of H_2O_2 generation. Therefore, it is evident that the most favorable scenarios are the following: carbon/PTFE/fabric, j = 59 mA cm^{-2} (Figure 10A), Q = 50 L h^{-1}, resulting in $[H_2O_2]_{60\ min}$ = 152.4 mg L^{-1} (Y_{ST} = 0.91 g L^{-1} h^{-1}) (Figure S2A); carbon/PTFE/fabric, j = 46 mA cm^{-2} (Figure 10B), Q = 30 L h^{-1}, yielding $[H_2O_2]_{60\ min}$ = 76.8 mg L^{-1} (Y_{ST} = 0.34 g L^{-1} h^{-1}) (Figure S2B); carbon/PTFE, j = 46 mA cm^{-2} (Figure 10 C), Q = 50 L h^{-1}, with $[H_2O_2]_{60\ min}$ = 98.3 mg L^{-1} (Y_{ST} = 0.43 g L^{-1} h^{-1}) (Figure S2C). It is therefore clear that for the reactor used, the optimal scenario with regard to electrochemical and fluid dynamics is obtained with carbon/PTFE/fabric, Q = 50 L h^{-1}, and j = 59 mA cm^{-2}.

The values of current efficiency and energy consumption (Figure 10) are within the same order of magnitude as those reported in ref 15. However, as mentioned earlier, it is worth noting that these parameters were determined in the present work using an experimental setup supplied with compressed air instead of pure oxygen, directly impacting the H_2O_2 concentrations and, consequently, the resulting values of Y_{ST}. Although the space-time yield range found in our study (0.22 g L^{-1} h^{-1} < Y_{ST} < 0.91 g L^{-1} h^{-1}) is in line with the range reported in ref 49 (0.21 g L^{-1} h^{-1} < Y_{ST} < 0.44 g L^{-1} h^{-1}) for particle-shaped electrodes in a fluidized bed electrochemical reactor and in ref 50 (Y_{ST} = 1.2 g L^{-1} h^{-1}) in a cyclone electrochemical reactor, showing the consistency of our findings with established and recent literature in the field of H_2O_2 generation by GDEs.

3.3. Flow Behavior in the Presence of Electrogenerated H_2O_2. To gain a deeper understanding of the hydrodynamics of H_2O_2 formation and its distribution within the reactor, simulations were carried out by varying the electrodes (carbon/PTFE/fabric and carbon/PTFE) and the hydrodynamic conditions (Q = 25 to 100 L h^{-1}). These simulations considered the interaction of H_2O_2 formed with the continuous phase in order to identify regions characterized by dead volume or short circuits resulting from the accumulation of H_2O_2 inside the reactor.

The H_2O_2 injection mass flow rates (kg s^{-1}) provided to Fluent were determined through experimental data (Figure 9) and calculated using mass balances, treating the reactor as the control volume. Consequently, the simulations considered the mass flow rates at the inlet and electrode, as indicated in Table S2. These simulations were performed using the transition SST micromixing model, which had previously been validated with experimental RTD data.

As illustrated in Figure 11, the variation in flow rate, from 50 L h^{-1} (Figure 11A) to 30 L h^{-1} (Figure 11B), and the change in electrode material, from carbon/PTFE/fabric (Figure 11A) to carbon/PTFE (Figure 11C), give rise to regions of low velocity fields with the development of dead zones, particularly noticeable at the reactor outlet for the flow rate of 30 L h^{-1} (Figure 11B) and in proximity to the carbon/PTFE electrode (Figure 11C). The simulation outcomes are in line with the experimental data, indicating a greater accumulation of H_2O_2 after 60 min for the carbon/PTFE/fabric configuration at 50 L h^{-1} (Figure 11A), where there is less occurrence of dead zones inside the reactor.

To investigate the influence of hydrodynamics on H_2O_2 accumulation, variations in the flow rate of fluid entering the reactor were explored, as illustrated in Figure 12. Proportional calculations were carried out on the mass flow rate of H_2O_2, and the SST transition micromixing model was employed. Notably, at lower volumetric flow rates, such as 25 and 30 L h^{-1}, the presence of dead zones becomes more pronounced (Figure 11A,B). On the other hand, when increasing the volumetric flow rate to 75 and 100 L h^{-1} (Figure 11D,E), a greater prevalence of preferential flow paths is observed. Consequently, a flow rate of 50 L h^{-1} emerged as the optimal condition, exhibiting a lower degree of nonideality in terms of H_2O_2 accumulation. This result is in line with the experimental data, establishing it as the most suitable condition for application in the reactor examined. In order to scale up the system effectively, various factors need to be considered, such as increasing the electrode size, expanding the number of electrodes in a stack, or incorporating several stacks into the system.[33] These factors play a key role in determining the feasibility and efficiency of implementing the findings on a larger scale, ensuring successful translation of the experimental and computational results into practical applications.

https://doi.org/10.1021/acs.iecr.4c02264
Ind. Eng. Chem. Res. 2024, 63, 18053−18066

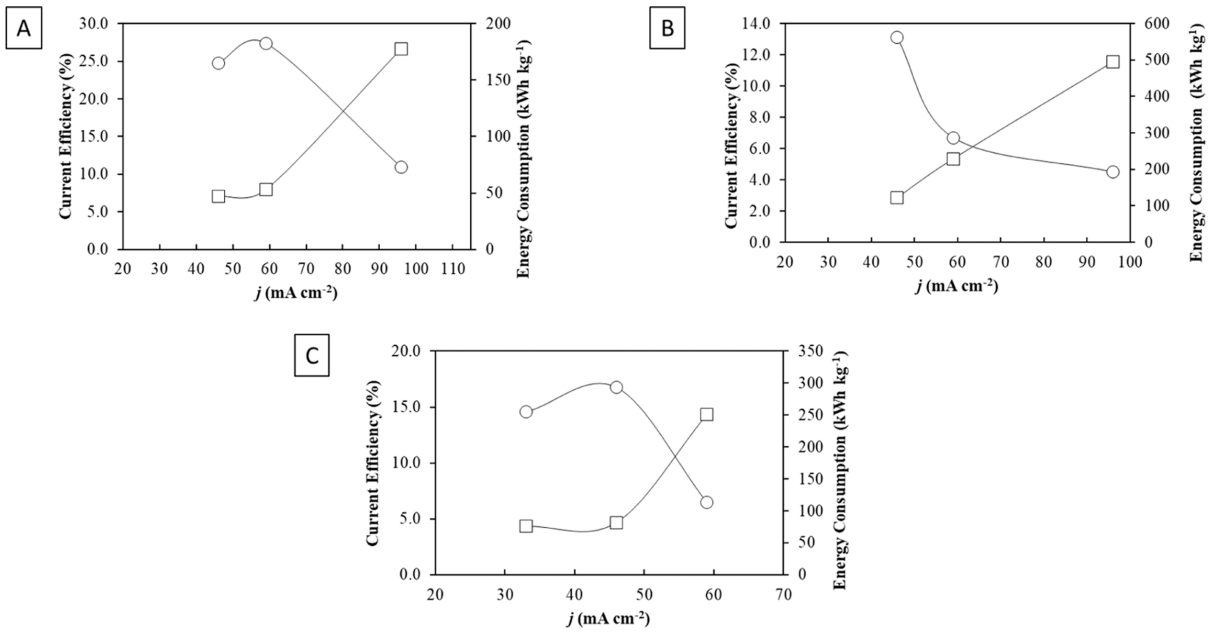

Figure 10. Comparison of current efficiency (circle) and energy consumption (square) at various current densities for H_2O_2 electrogeneration. (A) GDE: carbon/PTFE/fabric and Q = 50 L h^{-1}; (B) GDE: carbon/PTFE/fabric and Q = 30 L h^{-1}; (C) GDE: carbon/PTFE and Q = 50 L h^{-1}.

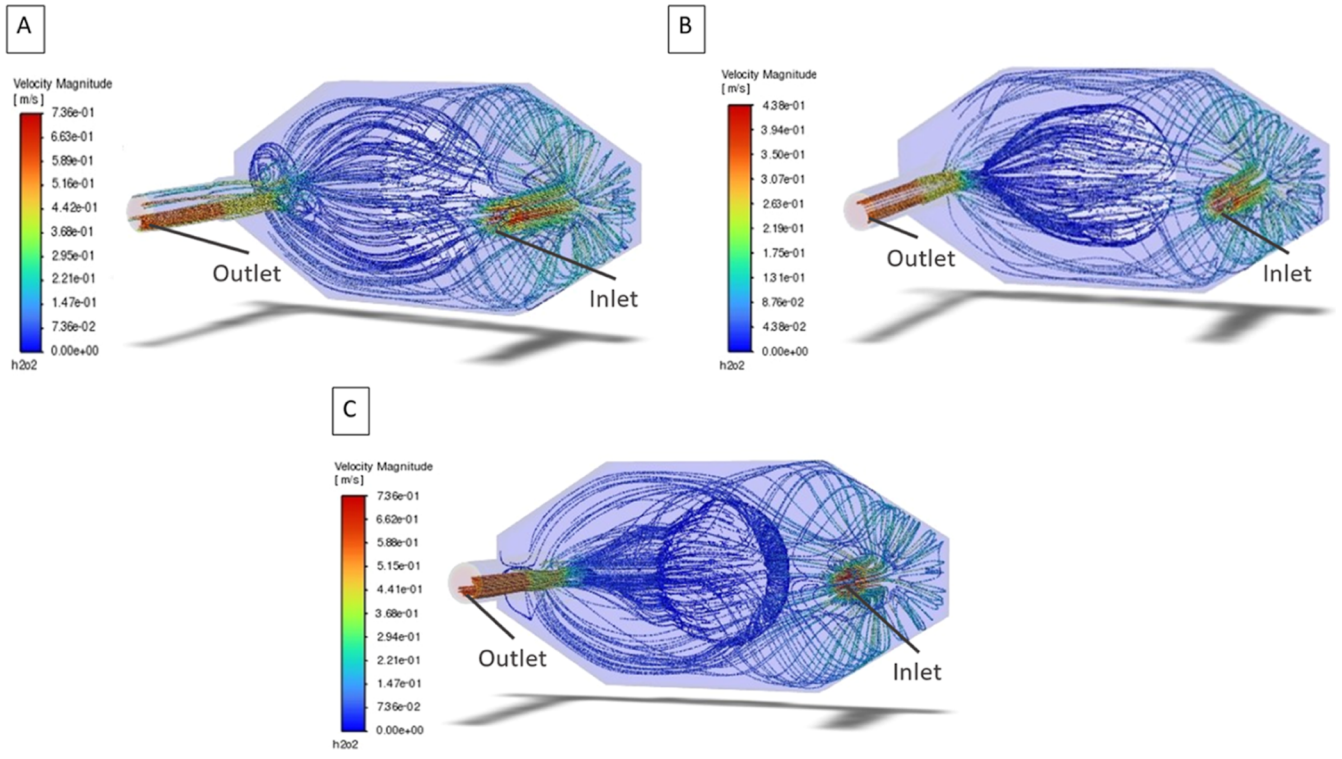

Figure 11. Particle tracking simulation of H_2O_2 distribution using different gas diffusion electrodes and hydrodynamic conditions. (A) Carbon/PTFE/fabric at 50 L h^{-1}; (B) carbon/PTFE/fabric at 30 L h^{-1}; (C) carbon/PTFE at 50 L h^{-1}.

4. CONCLUSIONS

This research has provided comprehensive insights into the intricate world of hydrodynamics within an electrochemical reactor with in situ H_2O_2 generation. The exploration encompassed a two-pronged approach, employing both macromixing and micromixing models to delve deeper into fluid dynamics.

The macroscopic perspective, especially the tanks-in-series (T-I-S) model, provided us with a qualitative comprehension of the fluid behavior within the confines of the reactor. On the other hand, from a microscopic point of view, based on the transition SST model, we have skillfully dissected the fluid dynamics, elucidating the formation of turbulence zones that characterize the system.

In terms of H_2O_2 electrogeneration and accumulation, the study revealed an interesting intersection between current

https://doi.org/10.1021/acs.iecr.4c02264
Ind. Eng. Chem. Res. 2024, 63, 18053−18066

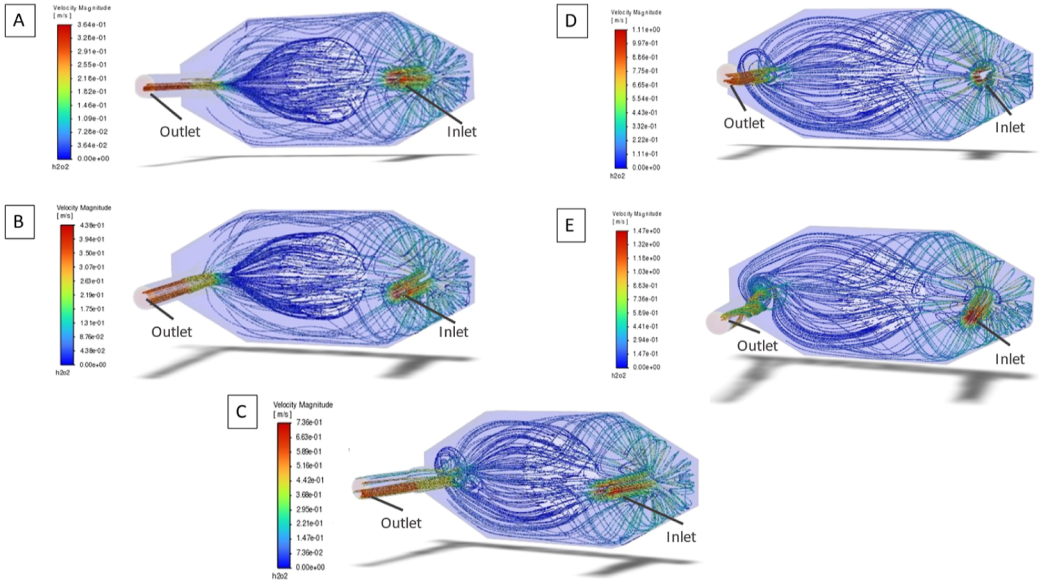

Figure 12. Particle tracking simulation of H_2O_2 distribution using carbon/PTFE/fabric at different flow rates. (A) $Q = 25$ L h^{-1}; (B) $Q = 30$ L h^{-1}; (C) $Q = 50$ L h^{-1}; (D) $Q = 75$ L h^{-1}; (E) $Q = 100$ L h^{-1}.

density, volumetric flow rate, and the type of gas diffusion electrode (GDE) configuration. The optimal operating point, identified experimentally for the carbon/PTFE/fabric configuration at 50 L h^{-1}, was corroborated by computational fluid dynamics (CFD) simulations. These simulations allowed us to visualize the distribution of H_2O_2 in the reactor volume, confirming the alignment between the experimental findings and simulation results.

Essentially, our findings shed light on the intricate interplay of factors governing H_2O_2 accumulation in an electrochemical reactor with gas diffusion electrodes, enriching the understanding of electrochemical reactor dynamics and offering valuable insights for future optimization endeavors.

■ ASSOCIATED CONTENT

Supporting Information

The Supporting Information is available free of charge at https://pubs.acs.org/doi/10.1021/acs.iecr.4c02264.

Sensitivity analysis, space-time yield, data used in CFD simulations, and mass flow rates (PDF)

■ AUTHOR INFORMATION

Corresponding Author

Antonio Carlos Silva Costa Teixeira − *Research Group in Advanced Oxidation Processes (AdOx), University of São Paulo, São Paulo, São Paulo 05508-010, Brazil; Department of Chemical Engineering, Escola Politécnica, University of São Paulo, São Paulo, São Paulo 05508-010, Brazil;* orcid.org/0000-0002-2790-2704; Email: acscteix@usp.br

Authors

Larissa Pinheiro de Souza − *Research Group in Advanced Oxidation Processes (AdOx), University of São Paulo, São Paulo, São Paulo 05508-010, Brazil; Department of Chemical Engineering, Escola Politécnica, University of São Paulo, São Paulo, São Paulo 05508-010, Brazil*

Isabela Matos Gaudio de Souza − *Research Group in Advanced Oxidation Processes (AdOx), University of São Paulo, São Paulo, São Paulo 05508-010, Brazil; Department of Chemical Engineering, Escola Politécnica, University of São Paulo, São Paulo, São Paulo 05508-010, Brazil*

Robson S. Souto − *São Carlos Institute of Chemistry, University of São Paulo, São Carlos, São Paulo 13560-970, Brazil*

Matheus Schiavon Kronka − *São Carlos Institute of Chemistry, University of São Paulo, São Carlos, São Paulo 13560-970, Brazil*

Bruno Ramos − *Department of Chemical Engineering, Centro Universitário da FEI, São Bernardo do Campo, São Paulo 09850-901, Brazil*

Marcos R. V. Lanza − *São Carlos Institute of Chemistry, University of São Paulo, São Carlos, São Paulo 13560-970, Brazil*

José Luís de Paiva − *Department of Chemical Engineering, Escola Politécnica, University of São Paulo, São Paulo, São Paulo 05508-010, Brazil*

Complete contact information is available at: https://pubs.acs.org/10.1021/acs.iecr.4c02264

Author Contributions

LP Souza: conceptualization, experimental investigation, data curation, formal analysis, simulation, and writing—original draft; IMG Souza: experimental investigation, data curation, formal analysis, and writing—original draft; RS Souto: experimental investigation, data curation, formal analysis, and writing—original draft; MS Kronka: experimental investigation, data curation, formal analysis, and writing—original draft; B Ramos: conceptualization, supervision, data curation, and writing—original draft; MRV Lanza: supervision, project administration, writing—original draft, and funding acquisition; JL Paiva: conceptualization, supervision, data curation, formal analysis, simulation, and writing—original draft; ACSC Teixeira: supervision, project administration, writing—original draft, and funding acquisition.

Funding

The Article Processing Charge for the publication of this research was funded by the Coordination for the Improvement

of Higher Education Personnel - CAPES (ROR identifier: 00x0ma614).

Notes

The authors declare no competing financial interest.

■ ACKNOWLEDGMENTS

The authors acknowledge the financial support provided by the following Brazilian funding agencies: Coordenação de Aperfeiçoamento de Pessoal de Nível Superior − Brasil (CAPES) − Finance Code 001, Brazilian National Council for Scientific and Technological Development—CNPQ (Grants #303943/2021-1, #311230/2020-2, and #309154/2023-5), and São Paulo Research Foundation—FAPESP (Grants #2022/12895-1 and #2022/14178-5). The authors would also like to thank Prof. Roberto Guardani, from the University of São Paulo (USP), for his support.

■ LIST OF SYMBOLS

a	specific electrode surface, $m^2\ m^{-3}$
C	concentration, mol L^{-1}
$C(t)$	tracer concentration, mol L^{-1}
E^0	standard electrode potential, V
E	electrode potential, V
$E(t)$	exit-age distribution function, min^{-1}
F	Faraday constant, C mol^{-1}
F_2	blending function, -
I	current, A
j	current density, mA cm^{-2}
M	molar weight, g mol^{-1}
P	pressure, Pa
Q	volumetric flow rate, L h^{-1}
s^3	skewness, min^3
S	strain rate of the flow, s^{-1}
t	time, min
t_m	mean residence time, min
t_p	peak time, min
t_c	time for the current to pass through the cathode, s
V	reactor volume, mL
V_e	electrolyte volume, L
x_p	particle position vector, -

■ GREEK

α_1	model constant, -
σ^2	variance, min^2
ρ	density, kg m^{-3}
τ	space time, min
μ	viscosity, m^2 s
μ_t	turbulent viscosity, m^2 s
$\overline{u}$	mean velocity, m s^{-1}
u'	fluctuating velocity, m s^{-1}
u	local velocity, m s^{-1}
v	inlet velocity, m s^{-1}
v_p	particle velocity, m s^{-1}
ω	specific dissipation rate

■ REFERENCES

(1) Siahrostami, S.; Villegas, S. J.; Bagherzadeh Mostaghimi, A. H.; Back, S.; Farimani, A. B.; Wang, H.; Persson, K. A.; Montoya, J. A Review on Challenges and Successes in Atomic-Scale Design of Catalysts for Electrochemical Synthesis of Hydrogen Peroxide. *ACS Catal.* **2020**, *10*, 7495−7511.

(2) Zhou, W.; Meng, X.; Gao, J.; Alshawabkeh, A. N. Hydrogen peroxide generation from O_2 electroreduction for environmental remediation: A state-of-the-art review. *Chemosphere* **2019**, *225*, 588−607.

(3) Cordeiro-Junior, P. J. M.; Kronka, M. S.; Goulart, L. A.; Veríssimo, N. C.; Mascaro, L. H.; Santos, M. C. D.; Bertazzoli, R.; Lanza, M. R. D. V. Catalysis of oxygen reduction reaction for H_2O_2 electrogeneration: The impact of different conductive carbon matrices and their physicochemical properties. *J. Catal.* **2020**, *392*, 56−68.

(4) Pang, Y.; Xie, H.; Sun, Y.; Titirici, M.-M.; Chai, G.-L. Electrochemical oxygen reduction for H_2O_2 production: catalysts, pH effects and mechanisms. *J. Mater. Chem. A* **2020**, *8*, 24996−25016.

(5) Santos, G. O. S. M.; Cordeiro-Junior, P. J.; Sánchez-Montes, I.; Souto, R.; Lanza, R. V. Recent advances in H_2O_2 electrosynthesis based on the application of gas diffusion electrodes: Challenges and opportunities. *Curr. Opin. Electrochem.* **2022**, *36*, 101124.

(6) Da Silva Souto, R.; Souza, L. P. D.; Cordeiro Junior, P. J. M.; Ramos, B.; Teixeira, A. C. S. C.; Rocha, R. D. S.; Lanza, M. R. V. Insights into Hydrodynamic and Operational Conditions for Scalable Hydrogen Peroxide Electrosynthesis Applications. *Ind. Eng. Chem. Res.* **2023**, *62* (37), 15084−15097.

(7) Gao, G.; Tian, Y.; Gong, X.; Pan, Z.; Yang, K.; Zong, B. Advances in the production technology of hydrogen peroxide. *Chin. J. Catal.* **2020**, *41*, 1039−1047.

(8) Ma, R.; Lin, G.; Zhou, Y.; Liu, Q.; Zhang, T.; Shan, G.; Yang, M.; Wang, J. A review of oxygen reduction mechanisms for metal-free carbon-based electrocatalysts. *npj Comput. Mater.* **2019**, *5*, 78.

(9) Wang, J.; Kong, H.; Zhang, J.; Hao, Y.; Shao, Z.; Ciucci, F. Carbon-based electrocatalysts for sustainable energy applications. *Prog. Mater. Sci.* **2021**, *116*, 100717.

(10) Garg, S.; Li, M.; Weber, A. Z.; Ge, L.; Li, L.; Rudolph, V.; Wang, G.; Rufford, T. E. Advances and challenges in electrochemical CO_2 reduction processes: an engineering and design perspective looking beyond new catalyst materials. *J. Mater. Chem. A* **2020**, *8*, 1511−1544.

(11) Perry, S. C.; Pangotra, D.; Vieira, L.; Csepei, L.-I.; Sieber, V.; Wang, L.; Ponce de León, C.; Walsh, F. C. Electrochemical synthesis of hydrogen peroxide from water and oxygen. *Nat. Rev. Chem.* **2019**, *3*, 442−458.

(12) Xie, J.; Jing, J.; Gu, J.; Guo, J.; Li, Y.; Zhou, M. Hydrogen peroxide generation from gas diffusion electrode for electrochemical degradation of organic pollutants in water: A review. *J. Environ. Chem. Eng.* **2022**, *10*, 107882.

(13) Kronka, M. S.; Fortunato, G. V.; Mira, L.; Dos Santos, A. J.; Lanza, M. R. V. Using Au NPs anchored on ZrO_2/carbon black toward more efficient H_2O_2 electrogeneration in flow-by reactor for carbaryl removal in real wastewater. *Chem. Eng. J.* **2023**, *452*, 139598.

(14) Barazorda-Ccahuana, H. L.; Fajardo, A. S.; Dos Santos, A. J.; Lanza, M. R. V. Decentralized approach toward organic pollutants removal using UV radiation in combination with H_2O_2-based electrochemical water technologies. *Chemosphere* **2023**, *342*, 140079.

(15) Costa, A. J. M.; Kronka, M. S.; Cordeiro-Junior, P. J. M.; Fortunato, G. V.; Dos Santos, A. J.; Lanza, M. R. V. Treatment of Tebuthiuron in synthetic and real wastewater using electrochemical flow-by reactor. *J. Electroanal. Chem.* **2021**, *882*, 114978.

(16) Lacasa, E.; Cañizares, P.; Walsh, F. C.; Rodrigo, M. A.; Ponce-de-León, C. Removal of methylene blue from aqueous solutions using an Fe^{2+} catalyst and in-situ H_2O_2 generated at gas diffusion cathodes. *Electrochim. Acta* **2019**, *308*, 45−53.

(17) Silva, T. O.; Fernandez-Cascán, J.; Isidro, J.; Saez, C.; Lanza, M. R.; Rodrigo, M. A. Degradation of real lindane wastes using advanced oxidation technologies based on electrogenerated hydrogen peroxide. *Process Saf. Environ. Prot.* **2023**, *180*, 535−543.

(18) Perry, S. C.; Ponce De León, C.; Walsh, F. C. Review—The Design, Performance and Continuing Development of Electrochemical Reactors for Clean Electrosynthesis. *J. Electrochem. Soc.* **2020**, *167*, 155525.

(19) Arenas, L. F.; Ponce De León, C.; Walsh, F. C. Critical review—The versatile Plane parallel electrode geometry: An illustrated review. *J. Electrochem. Soc.* **2020**, *167*, 023504.

https://doi.org/10.1021/acs.iecr.4c02264
Ind. Eng. Chem. Res. 2024, 63, 18053−18066

(20) Fogler, H. S. *Elements of Chemical Reaction Engineering*, 4th ed.; Prentice Hall, 2009.
(21) Colli, A. N.; Bisang, J. M. Study of the influence of boundary conditions, non-ideal stimulus and dynamics of sensors on the evaluation of residence time distributions. *Electrochim. Acta* **2015**, *176*, 463−471.
(22) Henquín, E.; Colli, A. N.; Bergmann, M. E. H.; Bisang, J. M. Characterization of a bipolar parallel-plate electrochemical reactor for water disinfection using low conductivity drinking water. *Chem. Eng. Process.* **2013**, *65*, 45−52.
(23) Rivera, F. F.; Hidalgo, P. E.; Castañeda-Záldivar, F.; Terol-Villalobos, I. R.; Orozco, G. Phenomenological behavior coupling hydrodynamics and electrode kinetics in a flow electrochemical reactor. Numerical analysis and experimental validation. *Chem. Eng. J.* **2019**, *355*, 457−469.
(24) Colli, A. N.; Bisang, J. M. Generalized study of the temporal behaviour in recirculating electrochemical reactor systems. *Electrochim. Acta* **2011**, *58*, 406−416.
(25) Colli, A. N.; Bisang, J. M. Evaluation of the hydrodynamic behaviour of turbulence promoters in parallel plate electrochemical reactors by means of the dispersion model. *Electrochim. Acta* **2011**, *56*, 7312−7318.
(26) Frías-Ferrer, Á.; Tudela, I.; Louisnard, O.; Sáez, V.; Esclapez, M. D.; Díez-García, M. I.; Bonete, P.; González-García, J. Optimized design of an electrochemical filter-press reactor using CFD methods. *Chem. Eng. J.* **2011**, *169*, 270−281.
(27) Gharibian, S.; Hazrati, H.; Rostamizadeh, M. Continuous electrooxidation of Methylene Blue in filter press electrochemical flow cell: CFD simulation and RTD validation. *Chem. Eng. Process.* **2020**, *150*, 107880.
(28) Rodríguez, A.; Rivera, F. F.; Orozco, G.; Carreño, G.; Castañeda, F. Analysis of inlet and gap effect in hydrodynamics and mass transport performance of a multipurpose electrochemical reactor: CFD simulation and experimental validation. *Electrochim. Acta* **2018**, *282*, 520−532.
(29) Vázquez, A. I.; Almazán, F. J.; Cruz-Diaz, M.; Delgadillo, J. A.; Lázaro, M. I.; Ojeda, C.; Rodríguez, I. Characterization of a Multiple-Channel Electrochemical Cell by Computational Fluid Dynamics (CFD) and Residence Time Distribution (RTD). *ECS Trans.* **2010**, *29*, 215−223.
(30) Li, Y.; Zhang, Y.; Xia, G.; Zhan, J.; Yu, G.; Wang, Y. Evaluation of the technoeconomic feasibility of electrochemical hydrogen peroxide production for decentralized water treatment. *Front. Environ. Sci. Eng.* **2021**, *15* (1), 1.
(31) Oloman, C.; Watkinson, A. P. Hydrogen peroxide production in trickle-bed electrochemical reactors. *J. Appl. Electrochem.* **1979**, *9*, 117−123.
(32) Walker, W. S.; Bezerra Cavalcanti, E.; Atrashkevich, A.; Fajardo, A. S.; Brillas, E.; Garcia-Segura, S. Mass transfer and residence time distribution in an electrochemical cell with an air-diffusion electrode: Effect of air pressure and mesh promoters. *Electrochim. Acta* **2021**, *378*, 138131.
(33) Walsh, F. C.; Arenas, L. F.; Ponce De León, C. Developments in plane parallel flow channel cells. *Curr. Opin. Electrochem.* **2019**, *16*, 10−18.
(34) Peres, J. C. G.; Silvio, U.; Teixeira, A. C. S. C.; Guardani, R. Study of an Annular Photoreactor with Tangential Inlet and Outlet: I. Fluid Dynamics. *Chem. Eng. Technol.* **2015**, *38*, 311−318.
(35) Moreira, J.; Bocalon Lima, V.; Athie Goulart, L.; Lanza, M. R. V. Electrosynthesis of hydrogen peroxide using modified gas diffusion electrodes (MGDE) for environmental applications: Quinones and azo compounds employed as redox modifiers. *Appl. Catal., B* **2019**, *248*, 95−107.
(36) Cordeiro-Junior, P. J. M.; Sáez Jiménez, C.; Vasconcelos Lanza, M. R. D.; Rodrigo Rodrigo, M. A. Electrochemical production of extremely high concentrations of hydrogen peroxide in discontinuous processes. *Sep. Purif. Technol.* **2022**, *300*, 121847.
(37) Wang, Y.; Sanly; Brannock, M.; Leslie, G. Diagnosis of membrane bioreactor performance through residence time distribution measurements — a preliminary study. *Desalination* **2009**, *236*, 120−126.
(38) Panizza, M.; Cerisola, G. Direct And Mediated Anodic Oxidation of Organic Pollutants. *Chem. Rev.* **2009**, *109*, 6541−6569.
(39) Fluent Inc. *Ansys Fluent User's Guide*, 2022.
(40) Du, Y.; Chen, X.; Li, S.; Berrouk, A. S.; Ren, W.; Yang, C. Revisiting a large-scale FCC riser reactor with a particle-scale model. *Chem. Eng. Sci.* **2022**, *249*, 117300.
(41) Du, Y.; Li, S.; Chen, X.; Li, Y.; Wang, B.; Yang, C. A novel methodology to construct compartment models for a circulating fluidized bed riser. *Chem. Eng. Sci.* **2023**, *269*, 118470.
(42) Bai, H.; Stephenson, A.; Jimenez, J.; Jewell, D.; Gillis, P. Modeling flow and residence time distribution in an industrial-scale reactor with a plunging jet inlet and optional agitation. *Chem. Eng. Res. Des.* **2008**, *86*, 1462−1476.
(43) Hu, B.; Zhang, X.; Wang, Z.; Wang, Z.; Ji, Y. Hydraulic characteristics, residence time distribution, and flow field of electrochemical descaling reactor using CFD. *Processes* **2021**, *9*, 1896.
(44) Sikkandar, M. Y.; Begum, S. S. An investigation on flow dynamics in the electrochemical reactor for the treatment of pharmaceutical wastewater. *Desalin. Water Treat.* **2019**, *137*, 41−48.
(45) Fluent Inc. *Ansys Fluent Theory Guide*, 2022.
(46) Cordeiro-Junior, P. J. M.; Lobato Bajo, J.; Lanza, M. R. D. V.; Rodrigo Rodrigo, M. A. Highly efficient electrochemical production of hydrogen peroxide using the GDE technology. *Ind. Eng. Chem. Res.* **2022**, *61*, 10660−10669.
(47) Barros, W. R. P.; Ereno, T.; Tavares, A. C.; Lanza, M. R. V. In situ electrochemical generation of hydrogen peroxide in alkaline aqueous solution by using an unmodified gas diffusion electrode. *ChemElectroChem* **2015**, *2*, 714−719.
(48) Cordeiro-Junior, P. J. M.; Martins, A. S.; Pereira, G. B. S.; Rocha, F. V.; Rodrigo, M. A. R.; Lanza, M. R. D. V. Bisphenol-S removal via photoelectro-Fenton/H_2O_2 process using Co-porphyrin/Printex L6 gas diffusion electrode. *Sep. Purif. Technol.* **2022**, *285*, 120299.
(49) Abt, M.; Franzreb, M.; Jestädt, M.; Tschöpe, A. Three-phase fluidized bed electrochemical reactor for the scalable generation of hydrogen peroxide at enzyme compatible conditions. *Chem. Eng. J.* **2023**, *476*, 146465.
(50) Wei, J.; Liu, Y.; Wu, X. A cyclone reactor of electrochemical advanced oxidation processes using PbO_2 anode and H_2O_2 electro-synthesis cathode. *Water Res.* **2023**, *245*, 120629.

https://doi.org/10.1021/acs.iecr.4c02264
Ind. Eng. Chem. Res. 2024, 63, 18053−18066